frontiers | Frontiers in Marine Science

TYPE Original Research
PUBLISHED 23 January 2025
DOI 10.3389/fmars.2024.1476768

OPEN ACCESS

EDITED BY
Gilles Reverdin,
Centre National de la Recherche Scientifique (CNRS), France

REVIEWED BY
Xilin Xiao,
Xiamen University, China
Simona Retelletti Brogi,
National Institute of Oceanography and Applied Geophysics, Italy
Pandi Sudarsana Rao,
National Centre for Polar and Ocean Research (NCPOR), India

*CORRESPONDENCE
Monika Zabłocka
monika_z@iopan.pl

RECEIVED 06 August 2024
ACCEPTED 12 December 2024
PUBLISHED 23 January 2025

CITATION
Zabłocka M, Kowalczuk P, Stoń-Egiert J, Terzić E, Bournaka E and Palacz AP (2025) Tracing the origins and transformations of fluorescence dissolved organic matter within western and eastern Greenland's shelves: a comparative study. *Front. Mar. Sci.* 11:1476768. doi: 10.3389/fmars.2024.1476768

Tracing the origins and transformations of fluorescence dissolved organic matter within western and eastern Greenland's shelves: a comparative study

Monika Zabłocka[1]*, Piotr Kowalczuk[1], Joanna Stoń-Egiert[1], Elena Terzić[1,2], Evanthia Bournaka[3] and Artur P. Palacz[1]

[1]Institute of Oceanology Polish Academy of Sciences, Sopot, Poland, [2]Division for Marine and Environmental Research, Ruđer Bošković Institute, Zagreb, Croatia, [3]DHI, Hørsholm, Denmark

Differences in the composition and spatial distribution of Fluorescent Dissolved Organic Matter (FDOM) between western and eastern Greenland shelf waters reflect the interplay of distinct regional environmental drivers-such as glacial meltwater inputs and stratification effects – which shape local DOM processing and biogeochemical cycles. These contrasts provide unique opportunity to understand how Arctic coastal system responds to climatic changes. To investigate these dynamics, we assessed FDOM by an application of multivariate statistical method - Parallel Factor Analysis (PARAFAC) on samples collected in July 2021 and August 2022. The PARAFAC enabled the distinction of five components representing both humic-like (C1 ($\lambda_{Ex}/\lambda_{Em}$ 318/392), C2 ($\lambda_{Ex}/\lambda_{Em}$ 363(261)/445), C5 ($\lambda_{Ex}/\lambda_{Em}$ 399/513)) and protein-like (C3 (tyrosine) – $\lambda_{Ex}/\lambda_{Em}$ 267/305, (C4 (tryptophan) – $\lambda_{Ex}/\lambda_{Em}$ 285/345)) substances, showing variations between western and eastern shelves and across different water layers (surface, deep chlorophyll *a* maximum depth – DCM, and below it (i.e., in the West Slope Greenland Core water – WSGC, and in the core Polar Water - PW). The analysis showed that western DOM is almost equally composed of humic-like (51%) and protein-like (49%) substances, while the eastern shelf is dominated by protein-like FDOM (56%), indicating a stronger influence of autochthonous production in the east. The highest fluorescence intensity was measured of the protein-like component C3 in both eastern (PW layer) and western (DCM layer) shelves. In the surface waters of the western Greenland shelf we found a statistically significant ($p<0.001$), although relatively weak ($R = 0.27$) correlation between I_p and the total chlorophyll *a* concentration, *Tchla*. Derived values of spectral indices (HIX, BIX, and FI), and a ratio of fluorescence intensities of protein-like components to fluorescence intensities of humic-like components, I_p/I_h, indicated that the FDOM in analyzed water was predominantly autochthonous, characterized with low molecular weight and low-saturation aromatic rings. This findings provide new insights into FDOM composition in the Arctic under changing climatic conditions.

KEYWORDS

dissolved organic matter, absorbance, fluorescence, Arctic Ocean, Greenland shelf, PARAFAC

1 Introduction

The Arctic Ocean, including Greenland's eastern and western shelves, represents a dynamic environment where freshwater and seawater interactions shape the region's hydrography and biogeochemistry. Dissolved organic matter (DOM) plays a crucial role in these hydrographic and biogeochemical processes, serving as a significant carbon reservoir (Hansell and Carlson, 2015), binding essential metals needed for phytoplankton growth (Morel and Price, 2003) and shielding marine organisms from harmful UV radiation (Repeta, 2015). Changes in the carbon cycle can alter the exchange of carbon between ocean and atmosphere (Lønborg et al., 2020), potentially affecting Earth's climate over geological periods. Recent accelerated warming in the Arctic Ocean ecosystem (Rantanen et al., 2022; Gutiérrez et al., 2021), alongside with glacial melt, reduction in sea ice cover (Serreze and Stroeve, 2015; Granskog et al., 2018), increased precipitation and accelerated permafrost thawing, contributing to coastal erosion and water runoff from land (Kipp et al., 2018). The watersheds of the Arctic rivers contain a substantial reservoir of organic carbon constituting about 40% of the world's near-surface labile soil carbon inventory (Zimov et al., 2006), currently bound in permafrost (Vonk and Gustafsson, 2013). The thawing of permafrost and increased discharge from Siberian and North American rivers (Stedmon et al., 2011; Anderson and Amon, 2015) are expected to significantly elevate the organic carbon inputs into the Arctic Ocean. These fresher and DOM enriched Arctic Ocean water outflowing to Atlantic and Pacific Oceans could significantly alter the DOM biogeochemistry in outflow shelves.

Water exchange between the Arctic, the North Pacific and the North Atlantic ocean basins occurs through several gateways: the Barents Sea, Fram Strait, Canadian Arctic Archipelago, and the Bering Strait. The water flowing through the Fram Strait and the Canadian Arctic Archipelago directly impacts the Greenland's shelf and coastal waters. The Greenland Shelf features two hydrographically distinct regions with unique characteristics. The East Greenland Shelf (EGS) water is influenced by the East Greenland Current (EGC), which carries cold core Polar Water (PW) southward along the continental shelf and slope. The estimated net volume transport of EGC range from 3.7 to 11.1 Sv (Sv = 10^6 m3 s^{-1}) (de Steur et al., 2009, 2014, 2018). Despite the considerable width of the East Greenland Shelf, warm and saline Atlantic water intrudes into the shelf and fjords, significantly altering the vertical distribution of water masses (Karpouzoglou et al., 2022; Gjelstrup et al., 2022). These factors, compounded by freshwater from melting sea ice and the Greenland Ice Sheet have led to the thinning of the core PW layer, and a shallowing of the Atlantic Water (AW) core, with a 1°C temperature increase since the 2000s' and marked decrease in salinity of surface waters on the East Greenland Shelf and the core of PW by 1.8 and 0.68, respectively, over the last two decades (Gjelstrup et al., 2022). The West Greenland Shelf (WGS) is primarily impacted by the West Greenland Current (WGC), which flows northward, currying the warmer West Greenland Slope Current (WGSW), and the offshore West Greenland Current (WGC), transporting the West Greenland Irminger Water (WGIW) (Aksenov et al., 2010). This water flows through the eastern part of the Davis Strait (Curry et al., 2014), following the continental shelf and slope in east Baffin Bay, with WGC tracing the west coast of Greenland. This region also sees the formation of transitional water (TrW). These waters flow into Labrador Sea, through Davis Strait, where the cumulative water transport was estimated at 2.6 ± 1 Sv, carrying a significant amount of fresh water (estimated at 92 ± 34 mSv (Beszczyńska-Möller et al., 2011) and contributing to water mass formation in the region (Curry et al., 2014).

DOM dynamics in these contrasting regions can be monitored effectively with optical methods (Granskog et al., 2012; Stedmon et al., 2015). A fraction of DOM, absorbs light in the ultraviolet and visible spectral ranges and it is called chromophoric dissolver organic matter – CDOM. Part of CDOM, called fluorescent dissolved organic matter – FDOM, has an ability to fluorescence absorbed energy. CDOM and FDOM are key optical constituents of seawater (apart from water molecules and particulate material suspended in the sea water), that influence light penetration and heat distribution in the water column (Pavlov et al., 2015; Granskog et al., 2015a, b).

The Excitation Emission Matrix (EEM) fluorescence spectroscopy technique, proposed by Traganza (1969), involves the measurements of emission spectra at a series of successively increasing excitation wavelengths. Coble (1996) assigned broad groups of organic compounds to specific spectral maxima with characteristic excitation and emission positions emerging at measured 3D landscapes. Multivariate statistical methods, such as the Parallel Factor Analysis (PARAFAC) (Stedmon et al., 2003), enabled an objective identification of different fluorophore classes underlying the EEMs signal, based on their excitation/emission maxima. This approach significantly advanced our understanding of production and degradation processes of DOM fluorophores across various marine and aquatic environments as well as in engineered water systems (Coble et al., 2014; Stedmon and Nelson, 2015 and references therein). This study aims to characterize the qualitative composition and spatial distribution of DOM optical properties on the East and West Greenland Shelves. By combining absorption and fluorescence spectroscopy methods with physical (temperature and salinity) and biological (chlorophyll a concentration) parameters, we seek to improve our understanding of how meltwater influx and autochthonous production alter DOM composition in these contrasting regions.

2 Materials and methods

2.1 Characterization of the study area

Greenland, is the world's largest island, which stretches between 59°N and 83°N latitude and 11°W and 74°W longitude. This location places the island at the confluence of major oceanic and atmospheric systems. Greenland is bordered by the Arctic Ocean to the north, the Greenland Sea to the east, the North Atlantic Ocean to the southeast, the Davis Strait to the southwest, Baffin Bay to the west, the Nares Strait and Lincoln Sea to the northwest, Figure 1. The island's extensive coastline and shelf areas are characterized by

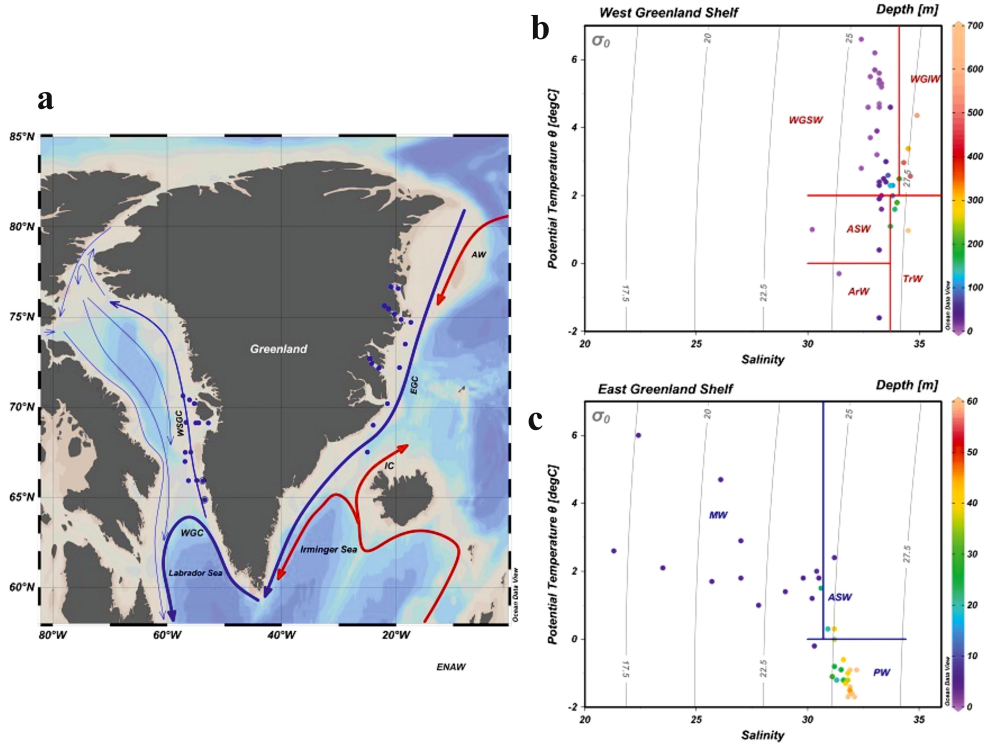

FIGURE 1
(A) Map of sampling stations on the west and east Greenland coasts along with the general circulation pattern. EGC – East Greenland Current, WGC – West Greenland Current, WSGC – West Surface Greenland Current, IC – Irminger Current, AW – Recirculated Atlantic Water. Water masses – T-S diagrams for all the oceanographic stations sampled in western **(B)** and eastern **(C)** Greenland with the identified water masses: core Polar Water (PW), West Greenland Shelf Water (WSGW), West Greenland Irminger Water (WGIW), Transitional Water (TrW), Arctic Surface Water (ASW), Arctic Water (ArW) (adapted from Tang, 2004; Curry et al., 2014). Gray lines indicate isopycnals (potential density – kgm^{-3})(created in Ocean Data View - Schlitzer R., 2022).

diverse and complex marine environments. The eastern and western shelf waters of Greenland, in particular, are notable for their distinct hydrographic and biogeochemical regimes. These differences are primarily shaped by the interaction of Arctic water masses, as well as significant freshwater inputs from glacial melt and river runoff. The western shelf is influenced by the West Greenland Current (WGC), which transports warmer Atlantic waters northward, while the eastern shelf is predominantly influenced by the colder, fresher core Polar Water (PW) of the East Greenland current (EGC).

Based on temperature (T) and salinity (S) measurements, four major water masses were distinguished in the West Greenland sampled region (West Greenland Slope Water - WGSW, West Greenland Irminger Water - WGIW, Arctic Water - ArW and Transitional Water - TrW) and three in the East Greenland sampled region (core Polar Water – PW, Melt Water - MW and Arctic Surface Water – ASW, adapted from Tang, 2004; Curry et al., 2014). T-S diagrams, with marked water mass distinctions and water samples depths are shown in Figure 1, for the West Slope Greenland Core water – WSGC, and the core Polar Water - PW respectively. Water masses are characterized in Supplementary Table S1. The general thermohaline pattern on the West Greenland Shelf (WGS) reveals the presence of warm (T > 2°C) and salty (S around 33) water (WGSW) with a mild thermocline and halocline. The East Greenland Shelf, was characterized by the presence of MW at the surface, with higher T and lower S due to the predominant discharge from melting Greenland ice sheet and icebergs. The MW was diluting the PW, thereby forming a steep and relatively shallow thermocline and halocline (Figure 2).

2.2 Sample collection and processing

2.2.1 Sample collection

Water samples were collected during two expeditions: one in July 2021 aboard the Danish research vessel, r/v Dana, and the other in August 2022 aboard the German research vessel – r/v Maria S. Merian. Field work was carried out in the shelf and fjord waters, as indicated Figure 1. Water column samples were collected with a rosette water sampler system from Sea-Bird Electronics Inc., equipped with 24 Niskin bottles, each holding 12 litres. Samples were collected at three different depths: surface (5 m), the deep chlorophyll-a maximum (DCM) depth determined at each station from chlorophyll-a fluorometer signal, and below the DCM, as shown in Figure 2. In 2021, the depths sampled below DCM ranged from 60 to 470 m, whereas in 2022, these samples were taken at 60 m.

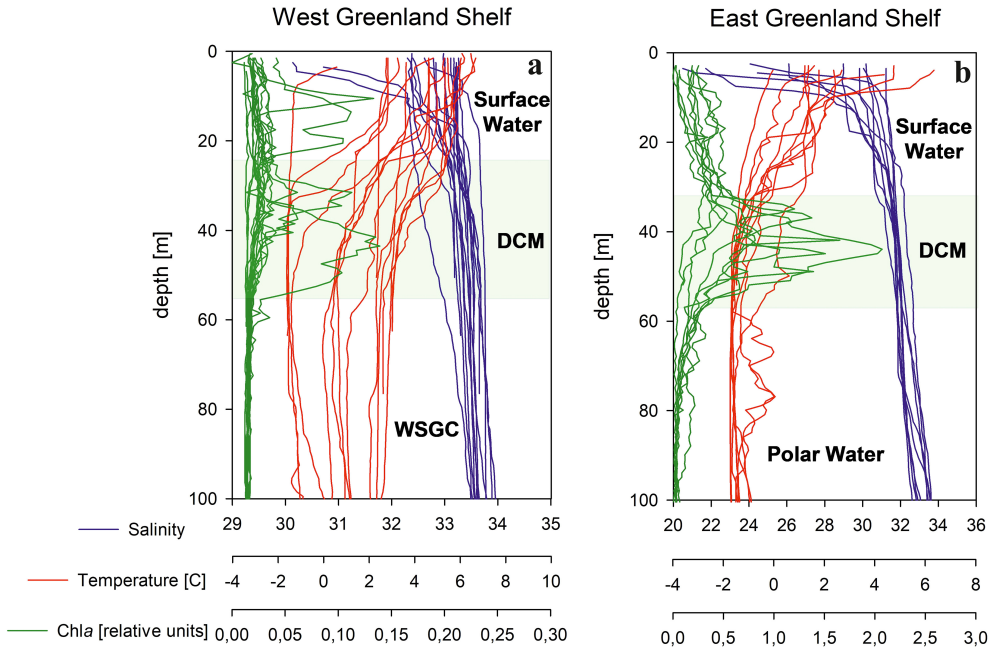

FIGURE 2
Vertical profiles of temperature, salinity and chlorophyll a concentration at **(A)** West and East **(B)** Greenland Shelf. DCM – deep chlorophyll a maximum layer, WSGC – West Slope Greenland Core water.

2.2.2 Sample processing

Samples collected for DOM absorption and fluorescence measurements were gravity filtered through an Opticap XL4 Durapore filter cartridge with a nominal pore size of 0.2 µm, directly attached to the Niskin bottle tap. To avoid sample contamination, both the cartridge filter and tubing were pre-treated with 10% HCL solution and rinsed with ultrapure MilliQ and the sample water before collection. All samples were then filtered into pre-combusted amber glass vials and stored at 4°C in dark, ensuring the preservation of DOM optical properties for several weeks (Stedmon and Markager, 2001).

Samples collected for high performance liquid chromatography (HPLC) pigment analysis were filtered using Whatman 25mm GF/F filters. The filter pads, with retained material, were immediately placed in liquid nitrogen and subsequently stored at -80°C until analyses.

2.2.3 CDOM absorption measurements

Measurements of CDOM absorbance were carried out using a double-beam Perkin-Elmer Lambda-650 spectrophotometer in the spectral range of 250–700 nm. Measurements were made in a 10-cm quartz cell, and the fresh ultrapure water was used as a reference. The CDOM absorption coefficient $a_{CDOM}(\lambda)$ was calculated using the equation:

$$a_{CDOM}(\lambda) = 2.303 \;\; A(\lambda)/l \qquad (1)$$

where: $A(\lambda)$, is the absorbance, l is the optical path length in meters, and the factor 2.303 is the natural logarithm of 10.

The CDOM absorption spectrum slope coefficient, $S_{300\text{-}600}$, was calculated in the spectral range 300 – 600 nm using a non-linear least squares fitting method with trust-region algorithm (Stedmon et al., 2000, 2003; Kowalczuk et al., 2006). The method, here implemented in Matlab R2013, uses the following equation:

$$a_{CDOM}(\lambda) = \; a_{CDOM}(\lambda_0)e^{-S(\lambda_0-\lambda)} + \; K \qquad (2)$$

where: λ_0 is 375 nm, and K is a baseline shift background constant resulting from residual scattering by fine size particle fractions, micro-air bubbles or colloidal material present in the sample, refractive index differences between sample and the reference, or attenuation not due to CDOM.

2.2.4 DOM fluorescence measurements and PARAFAC model

Fluorescence EEM spectra of collected DOM samples were measured with a HORIBA Aqualog spectrofluorometer in a 1 cm quartz cuvette. The excitation spectral range was set within 240–600 nm with a 3 nm increment. The emission spectral range was recorded between 246.65–829.44 nm with a 2.33 nm increment. The integration time was 8 s. All acquired EEM spectra were spectrally corrected with a set of instrument-dependent correction coefficients internally implemented within the spectrofluorometer.

The excitation and emission matrix spectra were processed using drEEM toolbox implemented in Matlab 2022a computing environment according to procedures described by Stedmon and Bro (2008) and Murphy et al. (2010, 2013). Spectrally corrected samples were calibrated and normalized against the Raman scatter

emission peak of the MilliQ water sample, run on the same day, excited at the wavelength of 351 nm and integrated in the spectral range 378 – 424 nm. The resulting EEM spectra were scaled in Raman units (R.U.). The samples were corrected for inner filter effects, using measured CDOM absorption spectra of corresponding water samples (section 2.2.3). The blank MilliQ water sample, corrected and calibrated in the same way as regular samples, was subtracted from each measured EEM to remove the Raman scattering signal. The PARAFAC model was applied to the data array with dimensions of 93 samples × 121 excitations × 153 emissions. It was run with a non-negativity constraint, assuming that signals from a complex mixture of DOM compounds can be separated and that the components differ from each other spectrally. The five-component model results were validated by the split-half validation technique (Harshman, 1984) applied to independent sub data sets (S4C6T3 – Splits, Combinations, Tests). The intensity of the n-th component in a given sample, IC_n, and the total fluorescence intensity, I_{tot}, were calculated using the equations (Kowalczuk et al., 2009):

$$IC_n = Score_n * Ex_n(\lambda_{max}) * m(\lambda_{max}) \quad (3)$$

where: $Score_n$ is the relative intensity ot the nth component, Ex_n (λ_{max}) is the maximum excitation loading of the nth component, $Em_n(\lambda_{max})$ is the maximum emission loading of the nth component derived from the model.

$$I_{tot} = \sum_1^n IC_n \quad (4)$$

2.2.5 HPLC measurements

Extraction pigments from cells were conducted by mechanical grinding and sonication (2 min, 20 kHz, Cole Parmer, 4710 Series) in dark conditionat 4 °C for 2 hours with the use of 90% acetone solution (Parsons et al., 1984). After centrifugation (20 min., 4 °C, 3210xg, Beckman, GS-6R) for the removal of filters and cellular debris, the extract was subjected to chromatographic analysis.

The chromatographic system HP1200 (Agilent, Perlan Technologies) is equipped with a diode array absorbance detector, a fluorescee detector and a C18 LichroCART™LiChrospher™ 100 RP18e (Merck) analytical column (with dimensions of 250 x 4 mm, particle size of 5 µm and pore size of 100 Å). The method used for pigments isolation and separation was introduced by Mantoura and Llewellyn (1983) and later modified by Stoń-Egiert and Kosakowska (2005). Pigments were separated in a gradient mixture of methanol, 1 M ammonium acetate and acetone. The detection of pigments was based on their retention time and absorbance spectra. The quantification was based on an external standardization equation combining chromatographic parameters of individual pigments with their concentration. The total chlorophyll-a concentration, *TChla*, was determined as the *sum of chlorophyll a, allomer chlorophyll a, epimer chlorophyll a, chlophyllide a, non-identified chlorophyll a derivatives.* The chromatographic system calibration was based on commercially available pigment standards (The International Agency for 14C Determination DHI Institute for Water and Environment in Denmark), whereas the documented measurement precision was 2.9% ± 1.5% with a recurrence error of 9.7% ± 6.4% (Stoń-Egiert et al., 2010).

2.2.6 Spectral indices

Spectral indices, essential for tracking the dynamics of DOM, its sources and processes, based on measured DOM absorption and fluorescence spectra were calculated to describe DOM compositional properties: i) humification index – HIX, according to Zsolnay et al. (1999), biological index – BIX, according to Huguet et al. (2009), and fluorescence index – FI, according to McKnight et al. (2001). Additionally a ratio between protein-like components intensities to the sum of humic-like components intensities was calculated following Kowalczuk et al., 2013:

$$I_p / I_h = \frac{I_{C3} + I_{C4}}{I_{C1} + I_{C2} + I_{C5}} \quad (5)$$

where I_{Cn} is the intensity of the respective component from C1 to C5 identified by the PARAFAC model. The spectral characteristics and their origins are explained in the Results section and are given in Table 1.

3 Results

3.1 Vertical distribution of temperature, salinity, and total chlorophyll a concentration on east and west Greenland shelves

Vertical profiles of T and S, on both the western and the eastern shelves of Greenland were characterized by an increase of S and a decrease in T with depth. Lowest S and highest T values were measured at the surface, while highest S and lowest T values were found at greater depths (Figure 2, Supplementary Figure S1, Supplementary Table S3). T and S differences between the eastern and the western Greenland shelves were evident in the range of measured values.

At the East Greenland Shelf, the surface layer salinity exhibited variations ranging from 21.3 to 31.2, with a median value of 27.8. Such low values of salinity indicates a significant influence from meteoric water sources, including the melting Greenland Ice Sheet, sea ice and precipitation (Dodd et al., 2012; Gonçalves-Araujo et al., 2016). The fresher water layer's thickness demonstrated a decrease from around 20 m in the fjords (S values were recorded at 30.9 at 20 m and 20.5 at 3 m at the ARF1 station in the Ardencaple Fjord) to just a few meters at the shelf, where S of 31.2 was measured at 3 m depth at the DSOW1 station (Figure 1). Additionally, the variability in S measurements decreased with increasing depth, oscillating by 0.5% around the median value of 31.9 at the core of PW. S levels in the western Greenland Shelf were consistently higher than those in the eastern side, ranging from 30.2 to 34.9, with median values of 32.8 at the surface layer, 33.2 in the DCM layer, and 33.8 at greater depths, Figure 2.

In terms of T, the water column in the eastern shelf was generally about 2 °C cooler compared to the western shelf of

10.3389/fmars.2024.1476768

TABLE 1 Ranges of variability, median and 1st and 3rd quartiles (Q_1, Q_3) of HIX, BIX and FI indexes and I_p/I_h ratio in different environments.

Samples description	HIX	BIX	FI	I_p/I_h
All Data				
range	0.390 – 3.877	0.777 – 1.484	1.161 – 1.505	0.427 – 3.800
median	1.568	0.943	1.303	0.940
Q_1,Q_3	1.027; 2.308	0.913; 0.981	1.258; 1.342	0.628; 1.435
N	91	91	91	91
West Greenland Shelf				
Surface water				
range	0.631 – 2.401	0.801– 1.071	1.251 – 1.391	0.593 – 1.938
median	1.369	0.916	1.330	1.019
Q_1,Q_3	1.086; 1.795	0.880; 0.956	1.291; 1.341	0.827; 1.381
N	19	19	19	19
DCM - deep Chlorophyll a maximum depth				
range	0.443 – 3.103	0.852– 1.240	1.161 – 1.505	0.449 – 2.348
median	1.529	0.968	1.344	0.975
Q_1,Q_3	1.089; 2.156	0.929; 0.992	1.298; 1.395	0.665; 1.355
N	17	17	17	17
WSCG				
range	0.617 – 2.916	0.859– 1.372	1.242 – 1.432	0.443 – 1.932
median	1.952	0.945	1.347	0.707
Q_1,Q_3	1.272; 2.315	0.925; 0.967	1.330; 1.382	0.583; 1.224
N	17	17	17	17
East Greenland Shelf				
Surface water				
range	0.452 – 2.949	0.777– 1.484	1.176 – 1.311	0.617 – 3.366
median	0.862	0.953	1.250	1.906
Q_1,Q_3	0.617; 1.403	0.917; 1.017	1.222; 1.271	1.270; 2.665
N	14	14	14	14
DCM – deep Chlorophyll a maximum depth				
range	1.006 – 3.746	0.858– 1.114	1.217 – 1.337	0.466 – 1.507
median	2.083	0.944	1.254	0.848
Q_1,Q_3	1.520; 3.132	0.910; 0.976	1.231; 1.305	0.562; 1.106
N	14	14	14	14
PW				
range	0.390 – 3.877	0.807– 1.163	1.244 – 1.323	0.427 – 3.800
median	2.755	0.932	1.278	0.648
Q_1,Q_3	1.589; 3.049	0.913; 1.038	1.257; 1.298	0.549; 1.078
N	10	10	10	10

N, number of observations.

Greenland. Highest T was measured in the meltwater layer, where it varied between -0.2 and 6.0 °C with a median of 1.8 ° C. A pronounced thermocline was observed between 10 to 20 m depth, where T sharply decreased to sub-zero values, reaching -0.9 °C at the DCM and nearly approached the freezing point (-1.6 °C) at the core of PW below 50 m depth (Supplementary Table S3, Figure 2). In the western shelf of Greenland, measured values were predominantly positive and noticeably higher than those measured in the eastern shelf, ranging from -1.6 °C to 6.6 °C. Negative temperatures were recorded only at 3 outermost profiles in the Davis Strait in DCM and WSCG). The median T values were 4.7 °C at the surface, 2.5 °C, at DCM, and 2.3 C, at greater depths, indicating that most of the shelf was occupied by WGSW which is consistent with findings of Gonçalves-Araujo et al. (2016).

Total chlorophyll *a* concentration, *Tchla*, values in EGS were very small, ranging from 0.049 mg m^{-3} in surface waters to 0.659 mg m^{-3} at DCM. Median *Tchla* values increased from surface (0.103 mg m^{-3}) to highest values at DCM (0.191 mg m^{-3}) and dropped sharply below that layer to the lowest median value (0.062 mg m^{-3}). On the western coast of Greenland, water for *Tchla* measurements was collected only at the surface layer. These waters were characterized by a much wider range of *Tchla* values, from 0.024 to 1.999 mg m^{-3}, with an almost five times higher median *Tchla* in comparison to surface waters in EGS (Supplementary Table S3).

3.2 Distribution of $a_{CDOM}(350)$ and FDOM components in the west and east Greenland shelf waters

The absorption of CDOM in the WGS waters was relatively low, with the CDOM absorption coefficient, $a_{CDOM}(350)$, varying from 0.115 to 0.404 m^{-1} (Figure 3, Supplementary Table S3). The highest median value of $a_{CDOM}(350)$ was observed in the surface waters (0.260 m^{-1}), the lowest in deeper waters below DCM layer (0.215 m^{-1}), and intermediate $a_{CDOM}(350)$ values were found around the DCM (0.232 m^{-1}). CDOM absorption in the EGS waters was approximately two times higher compared to CDOM absorption observed in the WGS. $a_{CDOM}(350)$ values in the EGS ranged from 0.170 to 0.551 m^{-1}, increasing steadily with depth. The median $a_{CDOM}(350)$ value in the surface melt water layer was 0.437 m^{-1} and reached 0.480 m^{-1} in the core of the PW.

The CDOM absorption slope coefficient, $S_{300\text{-}600}$, in the WGS ranged narrowly from 0.016 to 0.022 nm^{-1} and its median value did not change with depth significantly, and equalled to 0.019 nm^{-1} in respective water layers. Values of $S_{300\text{-}600}$ in the EGS waters were higher compared to WGS waters and ranged from 0.018 to 0.025 nm^{-1}. In the EGS, median $S_{300\text{-}600}$ values were the same in all distinguished water layers and equal to 0.021 nm^{-1}.

The PARAFAC model identified three components (C1, C2 and C5) characterized with excitation in UV and emission in the VIS part of the spectrum (referred to as humic-like components) and two characterized with excitation and emission in UV (referred to as protein-like components) (C3 and C4). Contour plots and the excitation and emission spectra loadings of identified components, together with the split-half validation results, are presented in Figure 4. Excitation and emission characteristics of the modelled components are listed in Table 1. The excitation/emission characteristic of component one (C1) ($\lambda_{Ex}/\lambda_{Em}$ 318/392) resemble the peak M described by Coble (1996) considered as the organic matter of marine origin. Component two (C2) ($\lambda_{Ex}/\lambda_{Em}$ 363(261)/445) has the spectral characteristics of two mixtures of organic matter of terrestrial origin described by Coble (1996) as peaks A and C. The last humic-like component (C5) ($\lambda_{Ex}/\lambda_{Em}$ 399/513) has the spectral characteristics of the soil fulvic acids described by Stedmon et al. (2011) as peak D. The excitation/emission characteristics of components three (C3) ($\lambda_{Ex}/\lambda_{Em}$ 267/305) and four (C4) ($\lambda_{Ex}/\lambda_{Em}$ 285/345) resemble the spectral characteristics of tyrosine and tryptophan, respectively, described by Coble (1996) as peaks B and T. Components identified in this study were compared with those obtained in different environments by other scientists and published in the OpenFluor open access spectral database (Murphy et al., 2014) (Supplementary Table S2). Bar graphs in Figure 5 (top panel) illustrate the average fluorescence intensity of each identified component in both WGS and EGS, further averaged for three depth ranges (surface, DCM and PW core) in both studied shelves (bottom panel). Statistical data describing the total fluorescence intensity, I_{tot}, as well as fluorescence intensities of the respective PARAFAC components, $I_{C1\text{-}C5}$, in the two regions and specified depth ranges are provided in Supplementary Table S3.

A consistent pattern of DOM composition was observed in samples collected both in the west and the east shelves of Greenland, with components ranked in the same order of abundance: $C3_p$ > $C1_h$ > $C4_p$ > $C2_h$> $C5_h$ (Figure 5), however the averaged DOM fluorescence intensities observed in the EGS were ca. 2 times higher compared to the WGS. The same pattern of ranking of identified FDOM-EEMs components was found in surface and deep-water layers in the WGS and in PW core in the EGS. The order of the average fluorescence intensities of identified components in the DCM in the WGS was: $C3_p$ > $C1_h$ > $C2_h$ = $C4_p$ > $C5_h$. In the EGS surface melt water layer, the order of fluorescence intensities of respective components was: $C3_p$ > $C4_p$ > $C1_h$ > $C2_h$ > $C5_h$, while in the DCM water layer, the components were ordered as follows: $C1_h$ > $C3_p$ > $C4_p$ > $C2_h$ > $C5_h$ (Figure 5) (Cx_h – humic-like components; Cx_p – protein-like components).

The range of variability of the total fluorescence intensity, I_{tot}, in WGS waters was found to be between 0.052 to 0.132 R.U. Median I_{tot} value was highest in DCM layer (0.076 R.U.), slightly lower in the surface water (0.075 R.U.), and lowest in the West Slope Greenland Core (WSGC) water (0.065 R.U.). The observed range of I_{tot} variability in EGS waters was within 0.099 to 0.376 R.U. Median I_{tot} value was highest in the surface meltwater layer (0.172 R.U.), the lowest at the PW core (0.127 R.U.), with an intermediate value in the DCM layer (0.131 R.U.).

Median values of fluorescence intensities of identified components (I_{C1}-I_{C5}) in respective water layers of the WGS were characterized by low variability (Supplementary Table S3, Figure 6). The Mann-Whitney U test confirmed no statistically significant differences between median I_{C1}-I_{C3} and I_{C5} values in vertical profiles, with the exception of I_{C4}. Differences in fluorescence intensity of the tryptophan-like component C4 were statistically significant between surface water (0.012 R.U.) and deep waters (0.009 R.U.), and between DCM (0.012 R.U.) and deep waters (0.009 R.U.).

10.3389/fmars.2024.1476768

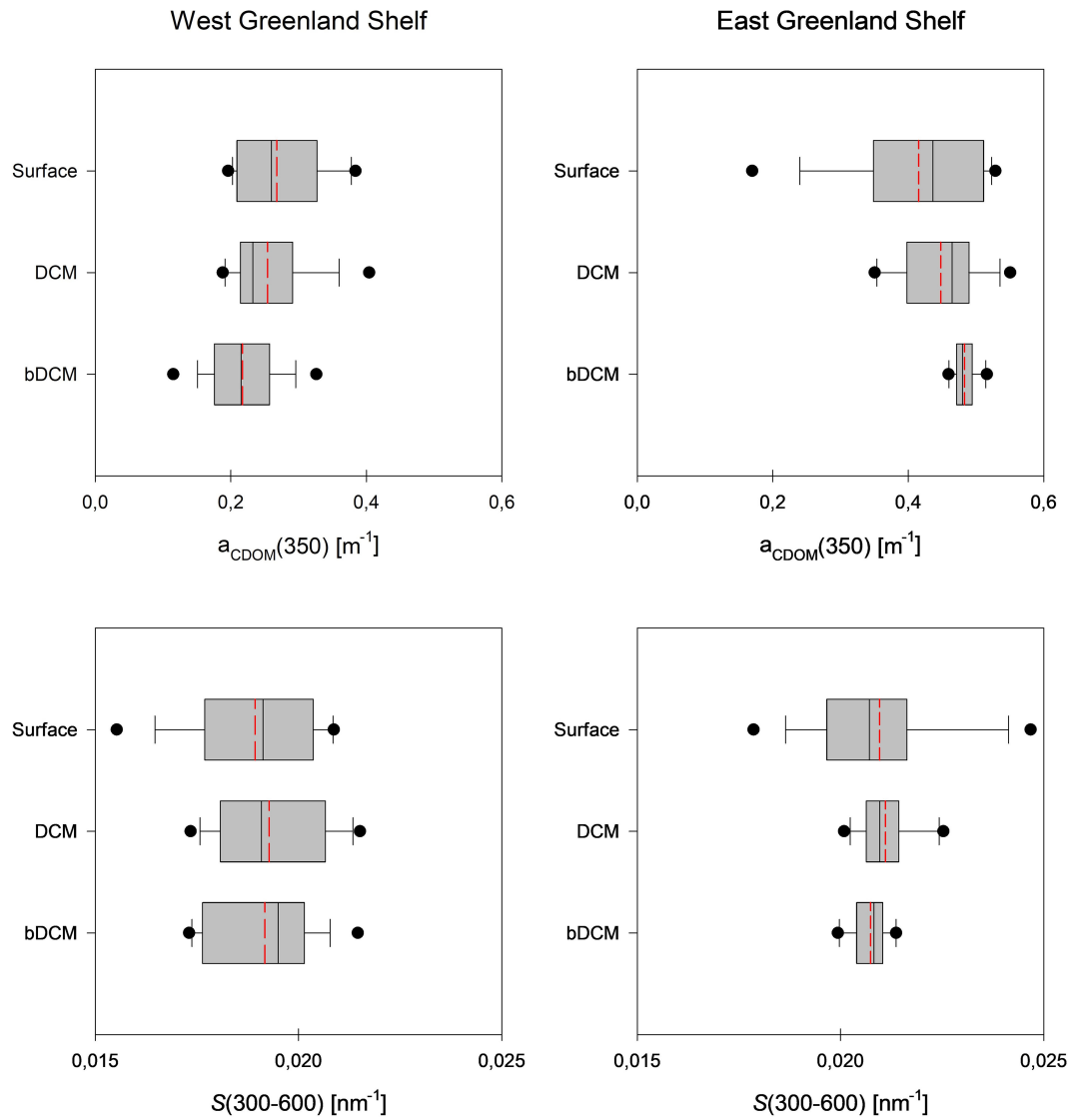

FIGURE 3
Vertical profiles of aCDOM (350) and $S_{300\text{-}600}$ on the West coast (2021) and east coast (2022) of Greenland. Median values are marked with the solid line, mean values are marked with the dashed red line, 10-th and 90-th percentiles are marked with the whiskers, and 25-th and 75-th percentiles with the box. The dots represent the outliers.

The vertical distribution of median values of fluorescence intensities of components I_{C1}-I_{C5} in the EGS waters was opposite to the one observed in the WGS (Supplementary Table S3, Figure 6). Median values of fluorescence intensity of components I_{C1}, I_{C2} and I_{C5} increased with depth and were the lowest in surface waters and the highest at the PW core. Observed differences in fluorescence intensity were statistically significant between surface melt water and DCM, and between melt water and core of the PW layers (the Mann-Whitney U test). Median values of fluorescence intensity of the tyrosine-like components C3 were highest in the surface meltwater layer and lowest at the PW core. The vertical distribution of median values of fluorescence intensity of component C4, I_{C4}, was similar to I_{C3}, where differences in observed values were statistically insignificant within respective water layers.

To better highlight FDOM compositional differences in the two contrasting outflow shelves, mutual proportion of fluorescence intensities of protein-like ($I_p = I_{C4} + I_{C3}$) and humic-like ($I_h = I_{C1} + I_{C2} + I_{C5}$) components were obtained. As presented in Figure 7, the protein-like components accounted for more than 50% of the total DOM fluorescence in surface waters (53%) and DCM (51%) layers of the WGS. The percent contribution of protein-like components to the total DOM fluorescence intensity in EGS surface waters and deep-water layers was higher than in the corresponding water layers at WGS: 66% and 52%, respectively. The lowest content of I_p was found in DCM layer at EGS (46%) (Figure 7).

3.3 Distribution of HIX, BIX and FI indexes and I_p/I_h ratio in the west and east Greenland shelf waters

Vertical profiles of the humification index (HIX), biological index (BI), fluorescence index (FI), and the ratio of respective

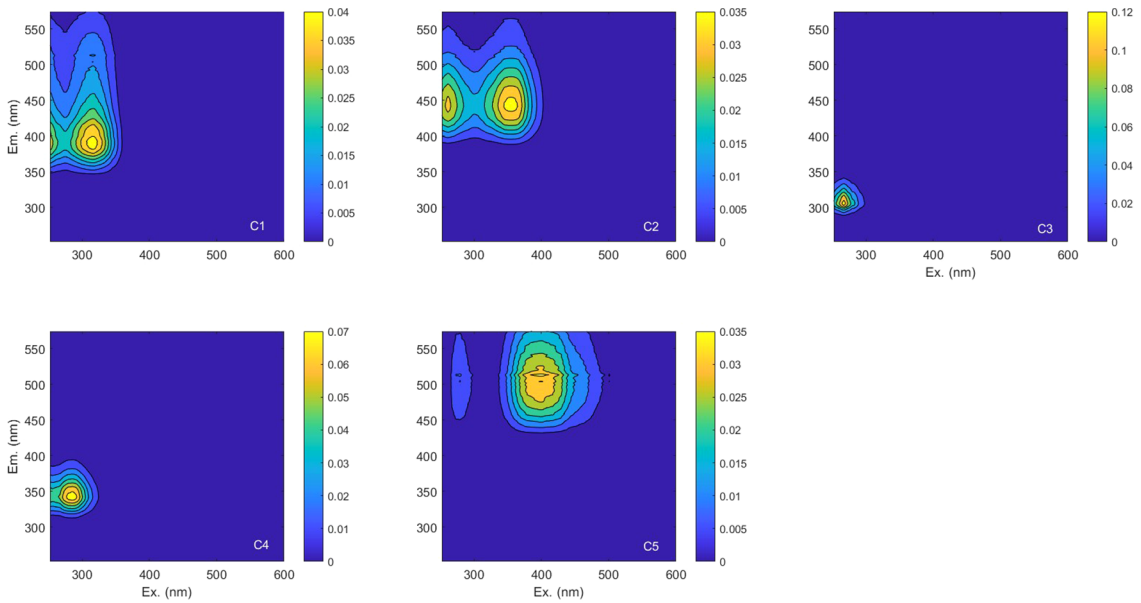

FIGURE 4
The PARAFAC model output showing fluorescence signatures of five components identified in the studied data set.

DOM fractions (I_p/I_h) in the WGS and EGS data sets are presented in Figure 8. The range of variability of HIX derived from samples collected in the WGS waters was from 0.31 to 3.10, with the highest median value observed in the WSGC water layer (1.95), the lowest in the surface layer (1.37), and intermediate in the DCM (1.53) (Table 1; Figure 8). Differences in median values found in respective water layers were not statistically significant. The range of variability of I_p/I_h in the WGS data set was from 0.44 to 2.35 and followed the opposite trend compared to HIX. The median value of I_p/I_h ratio was the highest in surface waters (1.02) and the lowest in the deep WSGC water layer (0.71) (Table 1; Figure 8). The same pattern as HIX (lowest values at the surface – 1.33, and highest values in deep waters – 1.35) characterized the distribution of median FI values, their range being from 1.16 to 1.51 (Table 1; Figure 8). The Mann-Whitney U test revealed that differences in median I_p/I_h and FI were statistically significant only at the surface and deep layers. The range of variability of the biological index, BIX, was from 0.80 to 1.37. Highest BIX median was found at the DCM (0.97), and the lowest in surface waters (0.92) of WGS. On the other hand, HIX values derived from samples collected in EGS waters were shifted towards higher values and ranged from 0.390 to 3.88, with a highest median value found at the PW core (2.76), and the lowest in the surface melt water layer (0.86), with intermediate values at the DCM (2.08) (Table 1; Figure 8). Differences in HIX values along the vertical profile were statistically significant. The vertical distribution patterns of I_p/I_h and FI in the EGS waters were similar to the ones at the WGS. The range of I_p/I_h variability in the EGS dataset was larger than at the WGS, from 0.43 to 3.80. The median vertical distribution of I_p/I_h values in the distinguished water layers was as follows: 1.91 – surface melt water, 0.85 – DCM, and 0.65 – PW core. The range of FI variability in EGS waters was 1.17 to 1.32 with median values steadily increasing with depth: 1.25 – surface water layer, 1.25 – DCM and 1.28 – PW core, respectively. The differences, although small, were statistically significant. The range of BIX variability in the EGS was wider than the one measured in the WGS and ranged from 0.78 to 1.48. The vertical distribution of the median BIX values in EGS was characterized by a decrease towards greater depths (0.95 – surface melt water, 0.94 – DCM, and 0.93 – PW core) (Table 1, Figure 8).

4 Discussion

4.1 The dynamics and distribution of DOM optical properties

The Arctic Ocean's dynamics of DOM optical properties are profoundly influenced by terrestrial inputs, particularly from the extensive river systems that discharge into its coastal margins. The highest CDOM absorption in the Arctic is observed along the Siberian Shelf, near its major rivers, where a_{CDOM} values in UVA range often exceed 10 m^{-1} (Gonçalves-Araujo et al., 2018; Juhls et al., 2019; Pugach et al., 2019; Drozdova et al., 2021). The Transpolar Drift transports Siberian riverine DOM from the central Arctic towards the Atlantic Ocean through Fram Strait (Granskog et al., 2012; Stedmon et al., 2015; Gonçalves-Araujo et al., 2020). By the time DOM reaches Greenland Selves, the Siberian-sourced CDOM/FDOM undergoes mixing and dilution by sea ice melt water (Gonçalves-Araujo et al., 2018) and transformed Atlantic water from Barents and Norwegian seas, which contain very low CDOM (Kowalczuk et al., 2017, 2019) and FDOM Makarewicz et al., 2018), and degradation through photo-bleaching (Stedmon et al., 2011; Granskog et al., 2012) that diminishes values of CDOM absorption coefficients and fluorescence intensity and making them more comparable to to those originating

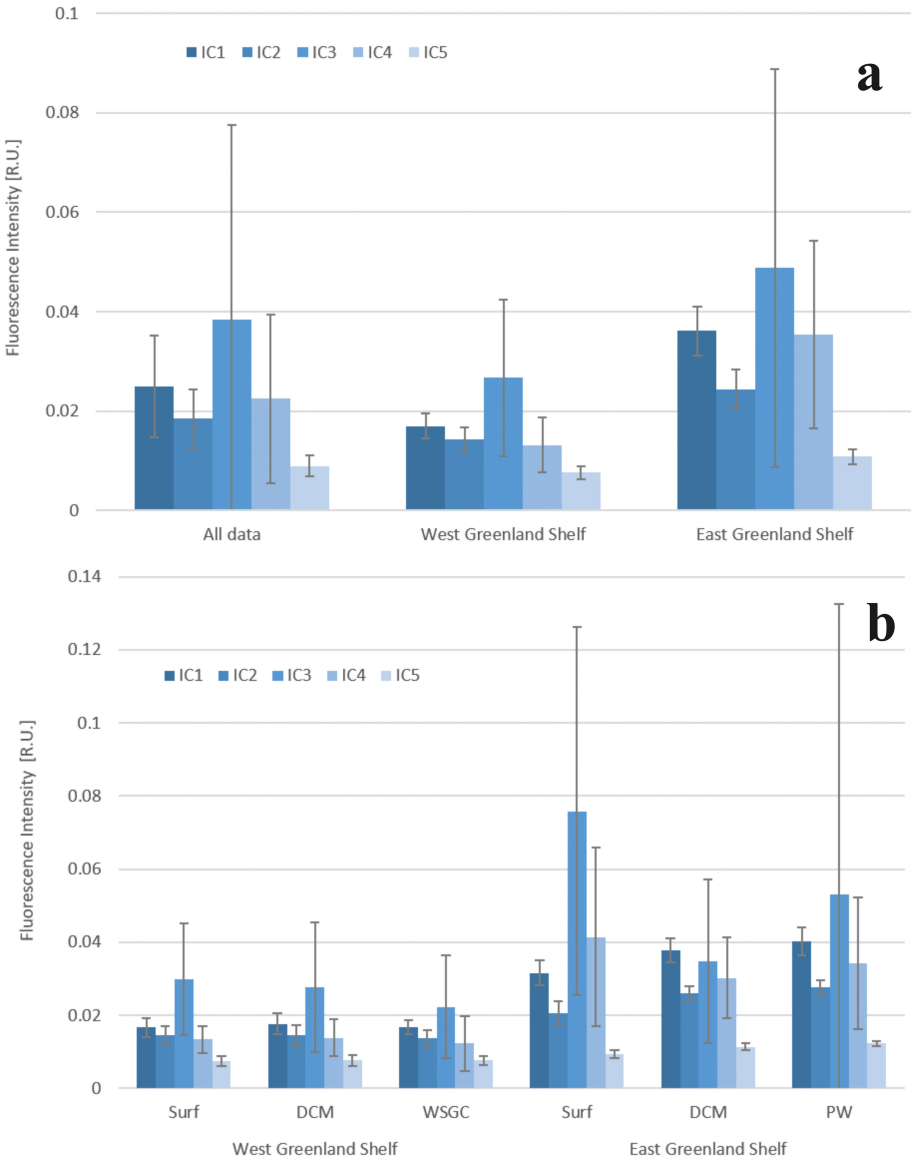

FIGURE 5
Fluorescence intensity of identified components C1-C5: in the whole data set and in WGS and the EGS **(A)** in three water layers: surface, DCM – deep chlorophyll a maximum and bDCM – below deep chlorophyll a maximum **(B)**. Bar plots represent and average values, the whiskers represent standard deviation.

from local sources. Water outflowing from the Hudson Bay, where $a_{CDOM}(355)$ may exceed 15 m^{-1} (Granskog et al., 2007), also serves as a notable source of DOM optical properties to Baffin Bay and Labrador Sea. However, its CDOM-rich waters are rapidly diluted in the Labrador Sea (Gueguen and Kowalczuk, 2014.

The overall CDOM/FDOM pattern across the Arctic Ocean determines higher DOM absorption and fluorescence intensity in EGS compared to WGS. This pattern is consistent with our study, where the $a_{CDOM}(350)$ values observed in EGS were approximately twice as high compared to those found in the WGS. This also indicated a varying degree of terrestrial DOM influence and water mass mixing between these regions. Values of $a_{CDOM}(350)$ reported here for the West and East Greenland Shelves closely match earlier reports, e.g., presented by Pavlov et al. (2015, in the EGS) and Gueguen and Kowalczuk, 2014, in the WGS, Baffin Bay and Davis Strait).

The analysis of temperature (T) and salinity (S) in the waters off the Greenland shelf reveals a complex interplay of water mixing processes and the impact of freshwater inputs from glacier melt and rivers discharge on the distribution of CDOM and FDOM.). These inputs, characterized by reduced salinity and fluctuating temperatures, contributed to the distinct spatial patterns of FDOM observed between the eastern and western shelves. In the EGS, the pronounced influence of freshwater is apparent through lower salinity levels, which significantly diluted CDOM/FDOM (Stedmon et al., 2015). This was especially seen in the coastal and fjords surface waters, especially lowering humic-like FDOM

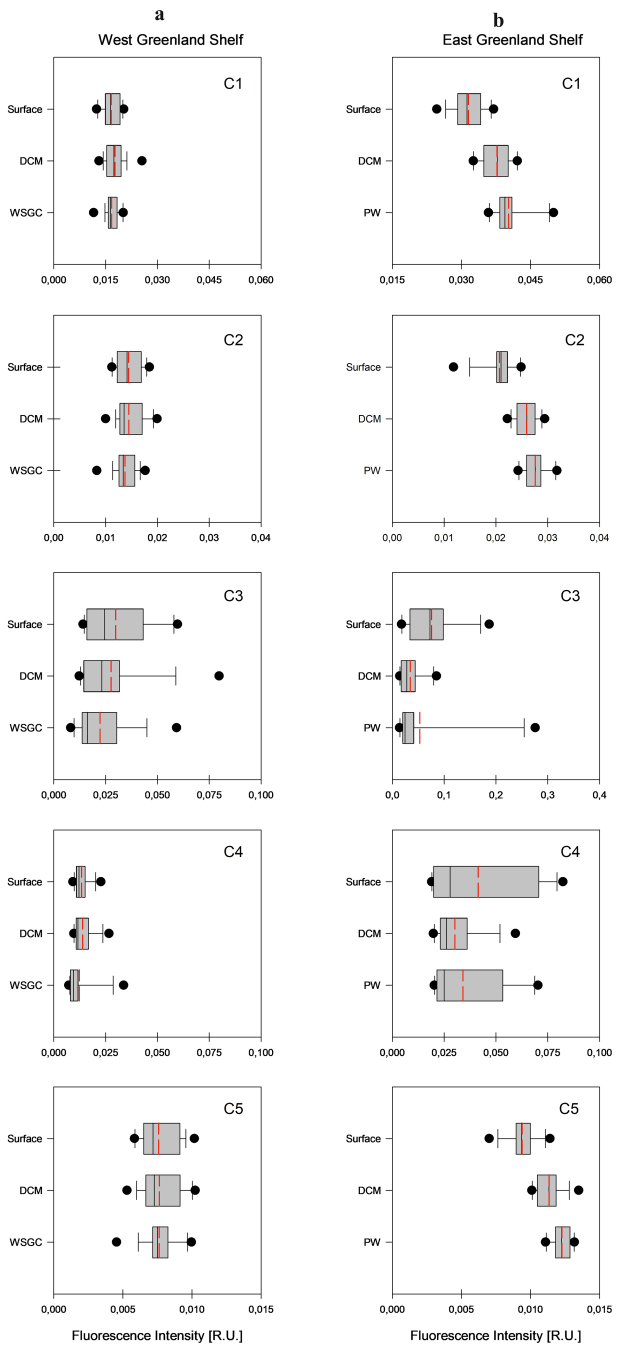

FIGURE 6
Vertical profiles of fluorescence intensity values of each identified component (C1-C5) in West Coast – 2021 data set **(A)** and in East Coast – 2022 data set **(B)**. Median values are marked with the solid line, mean values are marked with the dashed red line, 10-th and 90-th percentiles are marked with the whiskers, and 25-th and 75-th percentiles with the box. The dot represents the outliers.

intensities. The WGS experiences a greater influence from the warmer and saltier Atlantic waters, impacting FDOM composition with a higher presence of marine-derived protein-like components. In the surface layer, the absorption of CDOM and fluorescence intensity of FDOM are significantly modified by meltwater from sea ice or Greenland ice sheet, resulting in a positive relationship of these variables with increasing salinity (Granskog et al., 2012; Gonçalves-Araujo et al., 2016) (Figure 9). This impact is strongest in the EGS, while in the WGS, both CDOM and FDOM did not show any significant correlation with salinity. In surface and DCM water layers in the EGS, the fluorescence intensities of humic-like components decrease with decreasing salinity due to the dilution of core Polar Water fresher melt from glaciers containing lower concentration of humic substances. Protein-like substances did not show any trend with salinity.

The CDOM absorption spectrum slope coefficient ($S_{300\text{-}600}$), often regarded as a proxy for CDOM composition (Coble, 2007), showed small differences between the WSG and EGS, with median values of 0.019 nm^{-1} and 0.021 nm^{-1}, respectively. Although these differences suggest that variations in CDOM composition, influenced by physical and biological processes such as the mixing of water masses with contrasting DOM properties, autochthonous production, or microbial transformation, have had similar impacts on both shelves, a more probable conclusion is that $S_{300\text{-}600}$ coefficient exhibits limited sensitivity in resolving such variations. Consequently, DOM alteration cannot be effectively characterized solely based on spectral slope coefficient values. The $S_{300\text{-}600}$ median value observed in the EGS corresponded well to the spectral slope values observed at the marine impacted station in the Lena River delta in the Kara Sea, which is the one of the main CDOM/FDOM sources in the Eurasian basin of the Arctic Ocean. Average values of the CDOM absorption slope coefficient reported by Granskog et al. (2012) in the eastern Fram Strait were also 0.019 nm^{-1}, (calculated within a broader spectral range: 300-650 nm). In the eastern part of the Greenland Sea, Makarewicz et al. (2018) reported similar values in 2013 and 2015. Observations of $S_{350\text{-}600}$ reported by Kowalczuk et al. (2017) and Zabłocka et al. (2020) for open waters and under the ice water column north of Svalbard were much lower (0.015 nm^{-1} and 0.016 nm^{-1}, respectively) which suggested a predominantly autochthonous source of CDOM/FDOM in the Nansen Basin. The general compositional stability of CDOM in the Canada Basin has been confirmed by the multiyear observations reported by Dainard et al. (2019), who found stable values of the UV spectral slope coefficient $S_{275\text{-}295}$ in polar waters (ranging from 0.022 to 0.035 nm^{-1}). The observed stability of spectral slope values in Arctic waters, consistent with data reported in this region, points to a long-term stability in the composition of CDOM, and limited alteration by both autochthonous sources and photodegradation processes.

4.2 Comparative analysis of FDOM components in Arctic waters

The five PARAFAC components derived from the EGS and WGS databases and presented in this article have been previously reported in various aquatic environments. Components similar to C1 are typically associated with the *in situ* production, while components similar to C2 and C5 are considered to be of terrestrial origin. The presence of protein-like components (C3, C4) is an indicator of freshly produced DOM or degradation products of peptides (Yamashita and Tanoue, 2003). Total fluorescence intensities similar to those reported in our study

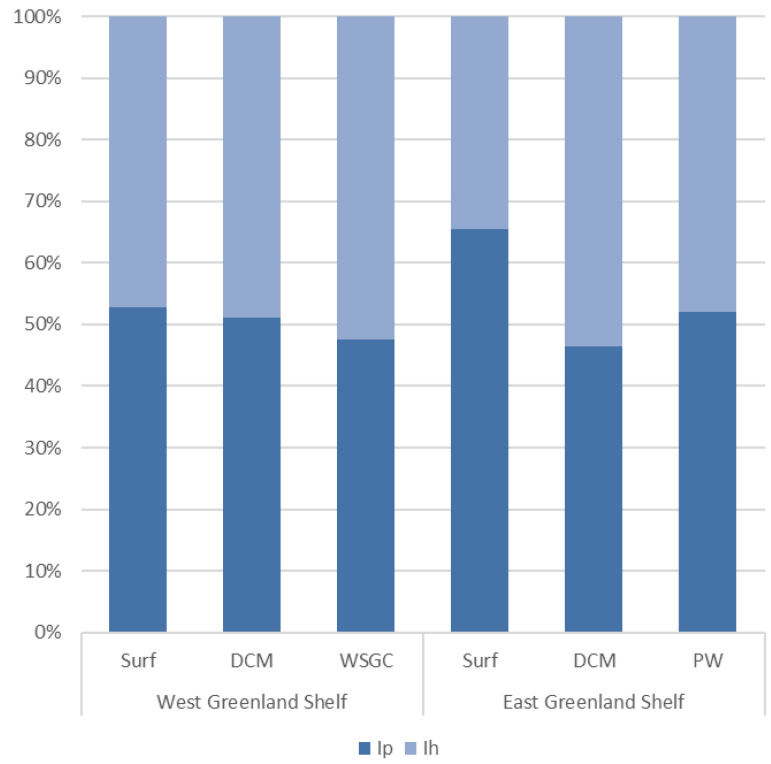

FIGURE 7
The FDOM composition in West and East Greenland Shelves in distinguished water layers (Surf, DCM,d WSGC and PW) expressed as the mutual proportion of fluorescence intensities of protein-like (I_p) and humic-like (I_h) components.

have been measured in the Canadian and European Arctic Ocean. Zabłocka et al. (2020) found that I_{tot} median values measured in water and sea ice samples collected north of Svalbard were ca. 50% lower than I_{tot} values reported in the current study in WGS waters and two and a half times lower compared to I_{tot} observed in EGS waters. Waters north of Svalbard (Zabłocka et al., 2020) were less abundant in protein-like than humic-like substances, as indicated by the I_p/I_h, which ranged from 0.013 to 1.610. In our study, in all water layers, corresponding I_p/I_h values were in the range of 0.43 to 3.80. It highlights that autochthonous production of FDOM plays a more significant role as a source of DOM in Greenland shelf waters compared to the waters north of Svalbard where main source of FDOM is transport from other regions. DeFrancesco et al. (2023) studied FDOM composition in the Canadian Basin over an 11-year period in five different water masses and reported median I_{tot} values similar to those measured in WGS waters. However, the percentage contribution of protein-like components to the total fluorescence intensities in the Canadian Basin did not exceed 21%. Gonçalves-Araujo et al. (2016) conducted research on both western (Davis Strait) and eastern (Iceland Sea) waters of Greenland, along with Fram Strait and distinguished three PARAFAC components (two humic-like and one protein-like). Fluorescence intensities of humic-like components reported by them were the highest in Fram Strait (Polar Water) and were similar to those measured in EGS in our study. The I_{C1} and I_{C2} values reported by Gonçalves-Araujo et al. (2016) in Davis Strait were similar to I_h values reported in this study in WGS. The protein-like fluorescence measurements in the same work reached 0.04 R.U., which is much lower compared to values in our study, I_p<=0.092 R.U. (WGS) and I_p<=0.297 R.U. (EGS). Gueguen and Kowalczuk (2014) sampled for optical properties of DOM in the Canadian Archipelago (CAA), Lancaster Sound, Baffin Bay and Labrador Sea (LS), and observed a reduction of terrestrial influence as waters move from CAA to LS. They reported values of total fluorescence intensities of PARAFAC components lower than those in our study (<0.1 R.U.).

In this study, we compared the quality and quantity of fluorescent DOM in two major pathways of water outflowing from the Arctic – the Western and Eastern Greenland shelves. Components with emission maxima in the UV-A spectral range (C3 and C4) are associated with compounds of lower aromaticity, such as dissolved amino acids embedded in proteins (Yamashita et al., 2003), and are often linked to aquatic productivity (Jørgensen et al., 2014). We found a correlation between chlorophyll *a* concentration (an indicator of biological activity) and the fluorescence intensity of the protein-like components (I_p) in surface waters on the WGS (Figure 10). The correlation coefficient value was low, R=0.27, but statistically significant (p<0.001), indicating that an autochthonous source could be an important driver of the FDOM variability. However, the direct impact of local FDOM production may be weakened by simultaneously occurring dilution by meltwater or uptake of protein-like FDOM fraction by microbial community, which effectively degraded the correlation between those variables. The correlation of I_p with *Tchla* in the EGS was weaker, perhaps due to very low *Tchla* values and very deep DCM depth. The highest

10.3389/fmars.2024.1476768

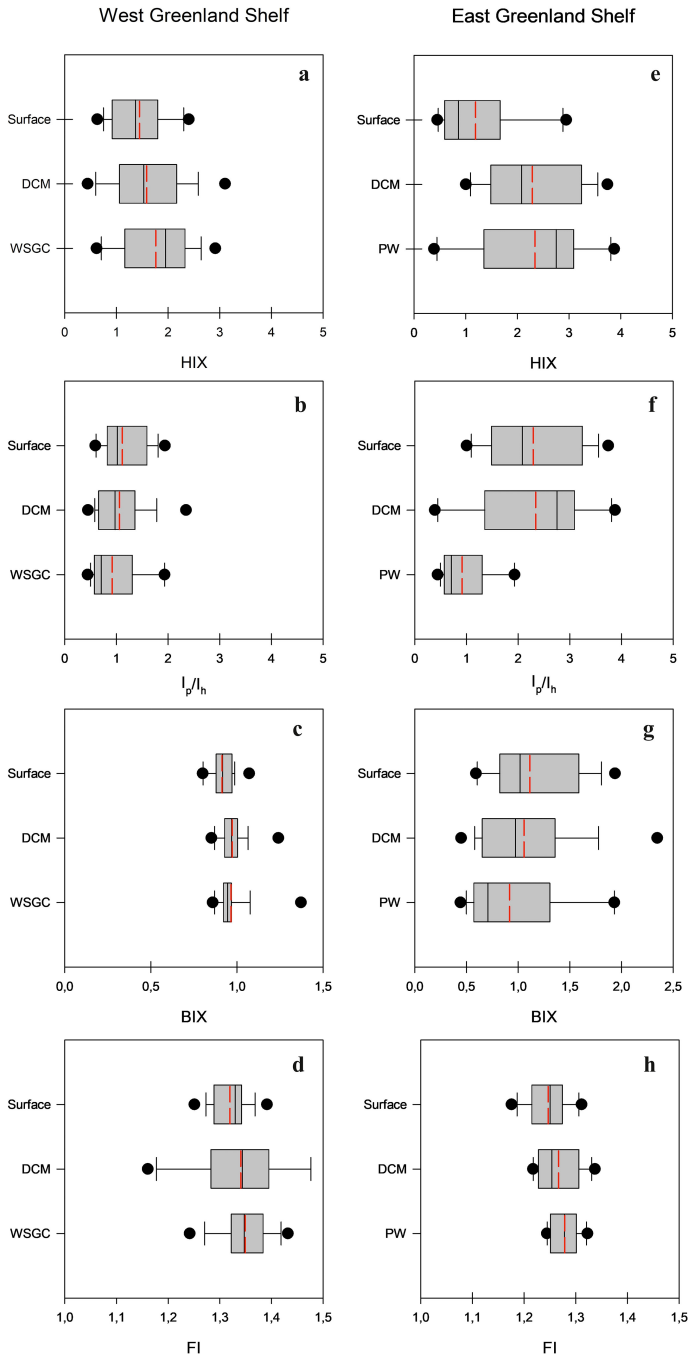

FIGURE 8
Vertical profiles of: the humification index, HIX **(A, E)**, the ratio of the respective DOM fractions, I_p/I_h **(B, F)**, the biological index, BIX **(C, G)** and the fluorescence index, FI **(D, H)** in West and East Greenland Shelves, accordingly. Median values are marked with solid line, mean values are marked with dashed red line, 10 th and 90 th percentiles are marked with the whiskers and 25 th and 75 th percentiles with the box. The dots represent the outliers.

FDOM intensity was observed in PW, and a significant part of the protein-like FDOM fraction was embedded in the wide array of organic compounds that make up DOM and are predominantly of terrestrial origin. Granskog et al. (2012) found a strong linear relationship between CDOM and the fraction of meteoric water in the PW in the Fram Strait and concluded that this was an indication of the riverine/terrigenous origin of CDOM in the East Greenland current.

4.3 Evaluating FDOM indices: insights into sources and transformation

We analysed four indices based on DOM fluorescence characteristics: the humification index (HIX), the biological index (BIX), the fluorescence index (FI), and the I_p/I_h ratio. Values of HIX are used to indicate the humification degree of FDOM and are strongly dependent on the C/H ratio in the molecular structure of DOM which

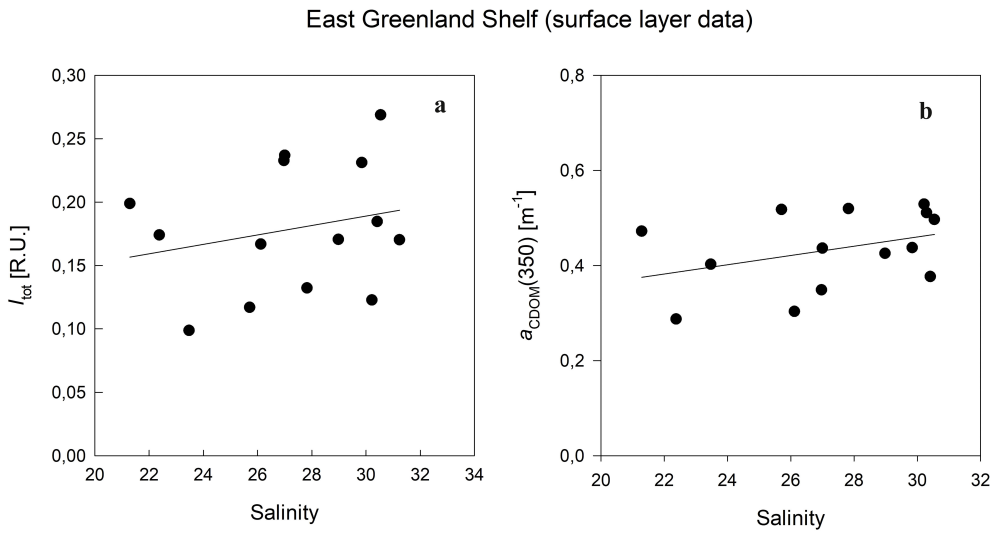

FIGURE 9
Relationship between the total fluorescence intensity (I_{tot}) and salinity **(A)**, and between CDOM absorption coefficient ($a_{CDOM}(350)$) and salinity **(B)** in surface waters of East Greenland Shelf.

increases with the aromaticity (Stubbins et al., 2014). High HIX (>10) is typical of freshwater environments, whereas values lower than 4 are usually found in marine waters dominated by autochthonous organic matter. When HIX is within 4 – 10, its character is of both terrigenous and marine origin (Huguet et al., 2009; Singh et al., 2010). In our study, HIX had values between 0.39 and 3.88, suggesting a biological or aquatic bacterial origin of DOM. Slightly higher HIX values were reported by Zabłocka et al. (2020) in Nansen Basin (Arctic Ocean). The median HIX value was comparable to that reported in the surface mixed layer water of the European continental shelf (Atlantic Ocean) (Kowalczuk et al., 2013). The fluorescence index, FI, exhibits a negative correlation with DOM aromaticity. Higher FI values signify stronger autogenesis of DOM, indicating a biological origin as a primary source of DOM. FI values exceeding 1.9 are characteristic of DOM produced by aquatic organisms, while values below 1.4 indicate an external source of DOM. Values falling in between suggest a combination of terrigenous and autochthonous DOM sources (McKnight et al., 2001). In our study, FI values ranged from 1.16 to 1.51. Within WGS, the highest median FI value was observed in WGSW (1.38), followed by slightly lower values in the DCM layer (1.34) and surface waters (1.330). A similar pattern was observed in EGS with the highest median FI in PW (1.28), the lowest in surface layer (1.25) and intermediate in DCM layer (1.25). These FI values indicate a lower influence of external sources in waters of WGS waters and a higher influence of external DOM transport on optical properties in the eastern shelf of Greenland.

The biological index, BIX, provides insights into the proportion of microbial-derived organic matter in comparison to exogenous organic matter. The higher the BIX value, the greater the share of DOM originating from biological sources, including phytoplankton and bacteria metabolic products. Conversely, low BIX values point at the terrestrial origin of DOM. Typically, BIX values in the range of 0.6 to 0.7 indicate a low autochthonous impact, values between 0.7 to 0.8 suggest intermediate autochthonous impact, while values in range of 0.9 to 1.0 signifies a strong autochthonous impact (Huguet et al., 2009; Wang et al., 2017b). In our study, BIX values ranged from 0.78 and 1.48. The lowest median BIX value was observed in surface waters of WGS (0.92), whereas the highest was in the DCM layer (0.97), also of WGS. Median BIX values in EGS were highest in surface waters (0.95), intermediate at the DCM layer (0.94) and the lowest in PW (0.93). These median values suggest mainly an autochthonous production of DOM.

The I_p/I_h ratio serves as a measure of the proportion between protein-like and humic-like FDOM components and was introduced by Kowalczuk et al. (2013), who established a certain regularity: areas characterized by a lower I_p/I_h ratio coincided with higher HIX values. A similar pattern was observed in the present study, where the I_p/I_h ratio ranged from 0.43 to 3.80. The lowest median I_p/I_h ratio was recorded in the PW in EGS (0.648) and in deep water in WSGC in the WGS (0.71). In contrast, the highest median I_p/I_h value (1.91) was measured in EGS surface waters and it was nearly twice as high as that measured for surface waters of WGS (1.02). The distribution of I_p/I_h clearly shows a higher contribution of protein-like fluorophores in the East Greenland Shelf surface waters, (almost four times higher I_p value than in WGS). This suggests that microbial decomposition is the primary source of protein-like components in those waters. Another factor contributing to the high I_p/I_h could be associated with the removal of humic-like fluorophores through photobleaching and dilution of sea water by melt water depleted with FDOM.

4.4 FDOM dynamics in eastern and western Greenland shelves

The eastern Greenland shelf is characterized by stronger stratification, lower salinity, and a shallower thermocline, primarily due to greater freshwater input from glacier melt and river runoff. These physical conditions limit vertical mixing, which

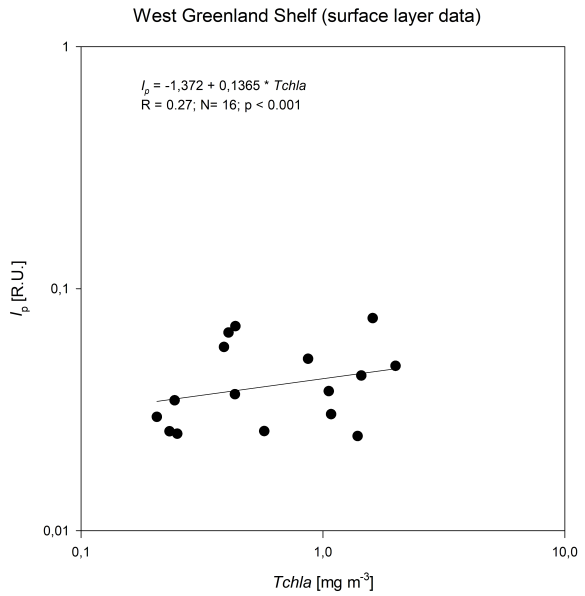

FIGURE 10
Relationship between the concentration of total chlorophyll a, Tchla, and the fluorescence intensity of protein-like components (I_p) identified by PARAFAC in surface waters of West Greenland Shelf.

in turn allows for a higher proportion of protein-like substances in the DOM, indicating strong autochthonous production dominated by microbial activity. The mixed layer depth (MLD) on the eastern Shelf ranged from 7 m to 18 m, with an average 9 m, while the depth of the deep chlorophyll a maximum (DCM) varied from 15 m to 48 m, averaging 33 m. Elevated BIX values, indicating the dominance of biologically derived DOM, and higher FI values, reflecting a significant microbial contribution to the DOM pool. Additionally, HIX values at greater depths point to the presence of terrestrial, humic-like DOM, brought in by glacial meltwater. Overall, the combination of strong stratification and limited mixing results in an eastern region that is heavily influenced by freshwater inputs and autochthonous microbial production.

In contrast, the western Greenland shelf experiences weaker stratification and greater vertical mixing, influenced by the influx of warmer, saltier Atlantic waters. The thermocline is deeper, and the DCM is more dynamic, which leads to a more balanced composition of DOM. This indicates a mix of terrestrial and marine sources of DOM. The MLD on the Western Shelf ranged from 9 m to 70 m, with an average of 16 m, while the DCM depth ranged from 8 m to 70 m, with an average of 35 m. The weaker stratification allows for the upward mixing of humic-like substances from deeper waters, contributing to a more complex DOM composition. HIX values are lower in the western shelf, suggesting less humified, autochthonous DOM in surface waters. The relatively balanced BIX values show that microbial production is present but less dominant compared to the eastern shelf, while the FI values similarly suggest a mixed DOM source. The influence of Atlantic water and increased mixing results in a western region that reflects a more intricate interplay of terrestrial inputs and autochthonous production, modulated by physical processes like vertical mixing and deeper thermocline dynamics.

5 Conclusions

Our study, based on samples from West Greenland Shelf (July 2021) and East Greenland Shelf (August 2022), has enabled us to characterize qualitative composition and spatial distribution of chromophoric and fluorescent dissolved organic matter (C/FDOM) in these waters. We identified five FDOM components: three humic-like (C1, C2, C5) and two protein-like (C3, C4). The Eastern Greenland shelf exhibited higher DOM fluorescence intensity and $a_{CDOM}(350)$ values compared to the West Greenland Shelf, indicating regional differences in DOM sources, advection and transformation processes. Surface waters of the East Greenland shelf were significantly enriched with protein-like substances, indicating a strong influence of autochthonous or microbial DOM origin. Optical indices: HIX, FI, BIX, and the I_p/I_h ratio, further underscores the dominant role of autochthonous or microbial DOM in the Eastern Greenland Shelf.

On the West Greenland Shelf, DOM composition showed small variation across water masses. In the East Greenland Shelf we have observed an increase in humic-like component contribution to DOM composition with depth and with the increasing presence of Polar Water. The weak correlation between chlorophyll a concentration and the fluorescence intensity of the protein-like components (I_p) in the WSG surface waters further supports the autochthonous DOM source.

The relative stability of the CDOM absorption spectrum slope coefficient in both Greenland Shelves over at least a decade suggests that our measurements can provide an adequate baseline for remote sensing applications, critical for developing reliable, basin-wide chlorophyll a estimates and monitoring of global ocean health.

Our findings underscore the importance of monitoring DOM in the context of tracing water masses. Particularly, the impact of sea ice and Greenland glacier melting on DOM dynamics in the coastal margins and fjords system should be investigated further. This study provides valuable insights into the DOM optical properties in the Greenland shelf waters, enhancing the understanding of biogeochemical processes in Arctic regions under changing climate.

Data availability statement

The raw data supporting the conclusions of this article will be made available by the authors, without undue reservation.

Author contributions

MZ: Conceptualization, Data curation, Formal analysis, Funding acquisition, Investigation, Supervision, Validation, Visualization, Writing – original draft, Writing – review & editing. PK: Investigation, Supervision, Writing – original draft, Writing – review & editing. JS-E: Data curation, Investigation, Writing – review & editing. ET: Data curation, Investigation, Writing – review & editing. EB: Data curation, Investigation, Writing – review & editing. AP: Funding acquisition, Investigation, Writing – review & editing.

Funding

The author(s) declare financial support was received for the research, authorship, and/or publication of this article. This work was supported by funding from the European Union's Horizon 2020 research and innovation program under grant agreement No 869383 (ECOTIP) and by the National Science Centre within the framework of project DOMinEA – Impact of hydrological regimes on the quantitative and qualitative optical properties of dissolved organic matter in West Spitsbergen fiords (contract no. UMO-2021/41/B/ST10/03603). PK was partially supported by National Science Centre within the framework of project (NCN) OPUS26, project OptiCal-Green (contract no. UMO-2023/51/B/ST10/01344).

Acknowledgments

We thank the crew of r/v Dana and r/v Merian for assistance in sampling during the two cruises.

Conflict of interest

Author EB was employed by company DHI.

The remaining authors declare that the research was conducted in the absence of any commercial or financial relationships that could be construed as a potential conflict of interest.

Publisher's note

Supplementary material

The Supplementary Material for this article can be found online at: https://www.frontiersin.org/articles/10.3389/fmars.2024.1476768/full#supplementary-material

References

Aksenov, Y., Bacon, S., Coward, A. C., and Holliday, N. P. (2010). Polar outflow from the Arctic Ocean: A high resolution model study. *J. Mar. Syst.* 83, 14–37. doi: 10.1016/j.jmarsys.2010.06.007

Anderson, L. G., and Amon, R. M. W. (2015). "DOM in the Arctic Ocean," in *Biogeochemistry of marine dissolved organic matter*, *2nd ed*. Eds. D. A. Hansell and C. A. Carlson Academic Press, 609–633.

Beszczynska-Möller, A., Woodgate, R. A., Lee, C., Melling, H., and Karcher, M. (2011). A synthesis of exchanges through the main oceanic gateways to the Arctic Ocean. *Oceanography* 24, 82–99. doi: 10.5670/oceanog.2011.59

Coble, P. G. (1996). Characterization of marine and terrestrial DOM in seawater usingexcitation–emission matrix spectroscopy. *Mar. Chem.* 51, 325–346. doi: 10.1016/0304-4203(95)00062-3

Coble, P. G. (2007). "Marine Optical Biogeochemistry: The Chemistry of Ocean Color. *Chem. Rev*. 107, 402–418. doi: 10.1021/cr050350+

Coble, P. G., Spencer, R. G. M., Baker, A., and Reynolds, D. M. (2014). "Aquatic Organic Matter Fluorescence," in *Aquatic Organic Matter Fluorescence*. Eds. P. G. Coble, J. Lead, D. M. Reynolds and R. G. M. Spencer (Cambridge University Press, Cambridge), 75–122.

Curry, B., Lee, C. M., Petrie, B., Moritz, R. E., and Kwok, R. (2014). Multiyear volume, liquid freshwater and sea ice transports through Davis Strait. *J. Phys. Oceanogr*. 44, 1244–1266. doi: 10.1175/JPO-D-13-0177.1

Dainard, P. G., Guéguen, C., Yamamoto-Kawai, M., Williams, W. J., and Hutchings, J. K. (2019). Interannual variability in the absorption and fluorescence characteristics of dissolved organic matter in the Canada Basin polar mixed waters. *J. Geophys. Res*. 124, 5258–5269. doi: 10.1029/2018JC014896

DeFrancesco, C., Gueguen, C., Williams, W. J., and Zimmermann, S. (2023). Interanual variability of fluorescent dissolved organic matter composition in Canada basin, Arctic Ocean from 2007 to 2017. *J. Geopchys. Res*. 128, 6.

de Steur, L., Hansen, E., Gerdes, R., Karcher, M., Fahrbach, E., and Holfort, J. (2009). Freshwater fluxes in the East Greenland Current: A decade of observations. *Geophysical Res. Lett.* 36, L23611. doi: 10.1029/2009GL041278

de Steur, L., Hansen, E., Mauritzen, C., Beszczynska-Möller, A., and Fahrbach, E. (2014). Impact of recirculation on the East Greenland Current in Fram Strait: Results from moored current meter measurements between 1997 and 2009. *Deep Sea Res. Part I: Oceanographic Res. Papers* 92, 26–40. doi: 10.1016/j.dsr.2014.05.018

de Steur, L., Peralta-Ferriz, C., and Pavlova, O. (2018). Freshwater export in the East Greenland Current freshness the North Atlantic. *Geophysical Res. Lett.* 45, 13359–13366. doi: 10.1029/2018GL08027

Dodd, P. A., Rabe, B., Hanses, E., Falck, E., Mackensen, A., Rohling, E., et al. (2012). The freshwater composition of the Fram Strait outflow derived from a decade of tracer measurements. *J. Geophys. Res.* 117 (C11). doi: 10.1029/2012JC008011

Drozdova, A. N., Nedospasov, A. A., Lobus, N. V., Patsaeva, S. V., and Shchuka, S. A. (2021). CDOM optical properties and DOC content in the largest mixing zones of the Siberian shelf seas. *Remote Sens.* 13, 114. doi: 10.3390/rs13061145

Gjelstrup, V. B., Sejr, M. K., Christiansen, J. S., Granskog, M. A., Koch, B. P., Møller, E. F., et al. (2022). Vertical redistribution of principle water masses on the Northeast Greenland Shelf. *Nat. Commun.* 2022, 7660. doi: 10.1038/s41467-022-35413-z

Gonçalves-Araujo, R., Granskog, M., Bracher, A., Zetsu-Scott, K., Dott, P. A., and Stedmon, C. A. (2016). Using fluorescent dissolved organic matter to trace and distinguish the origin of Arctic surface waters. *Sci. Rep*. 6, 33978. doi: 10.1038/srep33978

Gonçalves-Araujo, R., Rabe, B., Peeken, I., and Bracher, A. (2018). High colored dissolved organic matter (CDOM) absorption in surface waters of the central-eastern Arctic Ocean: Implications for biogeochemistry and ocean color algorithms. *PloS One* 13, e0190838. doi: 10.1371/journal.pone.0190838

Gonçalves-Araujo, R., Stedmon, C. A., de Steur, L., Osburn, C. L., and Granskog, M. A. (2020). A decade of annual Arctic DOC export with Polar Surface Water in the East Greenland Current. *Geophysical Res. Lett.* 47, e2020GL089686. doi: 10.1029/2020GL089686

Granskog, M. A., Fer, I., Rinke, A., and Steen, H. (2018). Atmosphere-ice-ocean-ecosystem processes in a thinner Arctic sea ice regime: The Norwegian Young Sea Ice (N-ICE2015) expedition. *J. Geophys. Res.-Oceans* 123, 3. doi: 10.1002/2017JC013328

Granskog, M. A., Macdonald, R. W., Mundy, C.-J., and Barber, D. G. (2007). Distribution, characteristics and potential impacts of chromophoric dissolved organic matter (CDOM) in Hudson Strait and Hudson Bay, Canada. *Cont. Shelf Res.* 27, 2032–2050. doi: 10.1016/j.csr.2007.05.001

Granskog, M. A., Nomura, D., Müller, S., Krell, A., Toyota, T., and Hattori, H. (2015a). Evidence for significant protein-like dissolved organic matter accumulation in Sea of Okhotsk sea ice. *Ann. Glaciol.* 56, (69). doi: 10.3189/2015AoG69A002

Granskog, M. A., Pavlov, A. K., Sagan, S., Kowalczuk, P., Raczkowska, A., and Stedmon, C. A. (2015b). Effect of sea-ice melt on inherent optical properties and vertical distribution of solar radiant heating in Arctic surface waters. *J. Geophys. Res.-Oceans* 120, 7028–7039. doi: 10.1002/2015JC011087

Granskog, M. A., Stedmon, C. A., Dodd, P. A., Amon, R. M. W., Pavlov, A. K., de Steur, L., et al. (2012). Characteristics of colored dissolved organic matter (CDOM) in the Arctic outflow in the Fram Strait: Assessing the changes and fate of terrigenous CDOM in the Arctic Ocean. *J. Geophys. Res.* 117, C12021. doi: 10.1029/2012JC008075

Gueguen, C., and Kowalczuk, P. (2014). "Colored dissolved organic matter in frontal zones," in *Chemical Oceanography of the frontal zones. Edition: the handbook of environmental chemistry*. Ed. I. Belkin (Springer, Berlin Heidelberg). doi: 10.1007/698_2013_244

Gutiérrez, J. M., Jones, R. G., Narisma, G. T., Alves, L. M., Amjad, M., Gorodetskaya, I. V., et al. (2021). "Atlas," in *Climate Change 2021: The Physical Science Basis.*

Contribution of Working Group I to the Sixth Assessment Report of the Intergovernmental Panel on Climate Change. Eds. V. Masson-Delmotte, P. Zhai, A. Pirani, S. L. Connors, C. Péan, S. Berger, N. Caud, Y. Chen, L. Goldfarb, M. I. Gomis, M. Huang, K. Leitzell, E. Lonnoy, J. B. R. Matthews, T. K. Maycock, T. Waterfield, O. Yelekçi, R. Yu and B. Zhou (Cambridge University Press, Cambridge, United Kingdom and New York, NY, USA), 1927–2058. doi: 10.1017/9781009157896.021

Hansell, D. A., and Carlson, C. A. (2015). *Biogeochemistry of Marine Dissolved Organic Matter*. *2nd ed*. Eds. D. A. Hansell and C. A. Carlson (Boston: Academic Press), xvii–xviii. doi: 10.1016/608B978-0-12-405940-5.09990-8

Harshman, R. A. (1984). "How can I know if it's 'real'? A catalog of diagnostics for use with three-mode factor analysis and multidimensional scaling," in *Research Methods for Multimode Data Analysis*. Eds. H. G. Law, J. Snyder, J. A. Hattie and R. McDonald (New York: Praeger), 566–591.

Huguet, A., Vacher, L., Relexans, S., Saubusse, S., Froidefond, J. M., and Parlanti, E. (2009). Properties of fluorescent dissolved organic matter in the Gironde Estuary. *Org. Geochem.* 40, 706–719. doi: 10.1016/j.orggeochem.2009.03.002

Jørgensen, L., Stedmon, C. A., Granskog, M. A., and Middelboe, M. (2014). Tracing the long-term microbial production of recalcitrant fluorescent dissolved organic matter in seawater. *Geophys. Res. Lett.* 41, 2481–2488. doi: 10.1002/2014GL059428

Juhls, B., Overduin, P. P., Hölemann, J., Hieronymi, M., Matsuoka, A., Heim, B., et al. (2019). Dissolved organic matter at the fluvial–marine transition in the Laptev Sea using in *situ* data and ocean colour remote sensing. *Biogeosciences* 16, 2693–2713. doi: 10.5194/bg-16-2693-2019

Karpouzoglou, T., de Steur, L., Smedsrud, L. H., and Sumata, H. (2022). Observed changes in the Arctic freshwater outflow in Fram Strait. *J. Geophysical Res.: Oceans* 127, 3. doi: 10.1029/2021JC018122

Kipp, S., Byrnes, W. C., and Kram, R. (2018). Calculating metabolic energy expenditure across a wide range of exercise intensities: the equation matters. *Appl. Physiol. Nutr. Metab.* 43, 639–642. doi: 10.1139/apnm-2017-0781

Kowalczuk, P., Meler, J., Kauko, H., Pavlov, A. K., Zabłocka, M., and Peeken, I. (2017). Bio–optical properties of Arctic drif ice and surface waters north of Svalbard from winter to spring. *J. Geophys. Res.– Oceans* 122, (6) 4634–466.

Kowalczuk, P., Sagan, S., Makarewicz, A., Meler, J., Borzycka, K., and Zabłocka, M. (2019). Bio-optical properties of surface waters in the Atlantic water inflow region off Spitsbergen (Arctic Ocean). *J. Geophys. Res.: Oceans* 124, 1964–1987. doi: 10.1029/2018JC014529

Kowalczuk, P., Tilstone, G. H., Zabłocka, M., Röttgers, R., and Thomas, R. (2013). Composition of Dissolved Organic Matter along an Atlantic Meridional Transect from fluorescence spectroscopy and Parallel Factor Analysis. *Mar. Chem.* 157, 170–184. doi: 10.1016/j.marchem.2013.10.004

Kowalczuk, P., Durako, M. J., Young, H., Kahn, A. E., Cooper, W.J., and Gonsior, M. (2009). Characterization of dissolved organic matter fluorescence in the South Atlantic Bight with use of PARAFAC model: Interannual variability. *Mar. Chem.* 113 (3–4), 182–196. doi: 10.1016/j.marchem.2009.01.015

Kowalczuk, P., Stedmon, C. A., and Markager, S. (2006). Modeling absorption by CDOM in the Baltic Sea from season, salinity and chlorophyll. *Mar. Chem.* 101, 1–11.

Lønborg, C., Carreira, C., Jickells, T., and Álvarez Salgado, X. A. (2020). Impacts of global change on ocean dissolved organic carbon (DOC) cycling. *Front. Mar. Sci.* 7. doi: 10.3389/fmars.2020.00466

Makarewicz, A., Kowalczuk, P., Sagan, S., Granskog, M. A., Pavlov, A. K., and Zdun, A. (2018). Characteristics of chromophoric and fluorescent dissolved organic matter in the Nordic seas. *Ocean Sci.* 14, 543–562. doi: 10.5194/os-14-543-2018

Mantoura, R. F. C., and Llewellyn, C. A. (1983). The rapid determination of algal chlorophyll and carotenoid pigments and their breakdown products in natural waters by reverse-phase highperformance liquid chromatography. *Anal. Chim. Acta* 151, 297–314. doi: 10.1016/S0003-2670(00)80092-6

McKnight, D. M., Boyer, E. W., Westerhoff, P. K., Doran, P. T., Kulbe, T., and Andersen, D. T. (2001). Spectrofluometric characterization of dissolved organic matter for indication of precursor organic material and aromacity. *Limnol. Oceanogr. Methods* 46, 1 38–1 48.

Morel, F. M. M., and Price, N. M. (2003). The biogeochemical cycles of trace metals in the oceans. *Science* 300, 944–947. doi: 10.1126/science.1083545

Murphy, K. R., Butler, K. D., Spencer, R. G. M., Stedmon, C. A., Boehme, J. R., and Aiken, G. R. (2010). Measurement of dissolved organic matter fluorescence in aquatic environments: an Interlaboratory comparison. *Environ. Sci. Technol.* 44, 9405–9412. doi: 10.1021/es102362t

Murphy, K. R., Stedmon, C. A., Graeber, D., and Bro, R. (2013). Fluorescence spectroscopy and multi–way techniques. *PARAFAC Anal. Methods-UK* 5, 6557. doi: 10.1039/c3ay41160e

Murphy, K. R., Stedmon, C. A., Wenig, P., and Bro, R. (2014). OpenFluor–an online spectral library of auto–fluorescence by organic compounds in the environment. *Anal. Methods-UK* 6, 658–661. doi: 10.1039/C3AY41935E

Parsons, T. R., Maita, Y., and Lalli, C. A. (1984). *A manual of chemical and biological methods for seawater analysis* (Oxford: Pergamon Press).

Pavlov, A. K., Granskog, M. A., Stedmon, C. A., Ivanov, B. V., Hudson, S. R., and Falk-Petersen, S. (2015). Contrasting optical properties of surface waters across the Fram Strait and its potential biological implications. *J. Mar. Sys.* 143, 62–72. doi: 10.1016/j.jmarsys.2014.11.001

Pugach, S. P., Pipko, I. I., Shakhova, N. E., Shirshin, E. A., Perminova, I. V., Gustafsson, Ö., et al. (2019). Dissolved organic matter and its optical characteristics in the Laptev and East Siberian seas: Spatial distribution and interannual variability, (2003–2011). *Ocean Sci.* 14, 87–103.

Rantanen, M., Karpechko, A., Lipponen, A., Nordling, K., Hyvarinen, K. R., Vihma, T., et al. (2022). The Arctic has warmed nearly four times faster than the globe since 1979. *Commun. Earth Environ.* 3, 168. doi: 10.1038/s43247-022-00498-3

Repeta, D. J. (2015). "Chemical Characterization and Cycling of Dissolved Organic Matter," in *Biogeochemistry of Marine Dissolved Organic Matter*. Eds. D. A. Hansell and C. A. Carlson (Academic Press, Amsterdam, Boston), 21–63. doi: 10.1016/B978-0-12-405940-5.00002-9

Schlitzer, R. (2022). Ocean data view. Available online at: http://www.odv.awi.de (Accessed November 11, 2023).

Serreze, M. C., and Stroeve, J. (2015). Arctic sea ice trends, variability and implications for seasonal ice forecasting. *Philos. Trans. A Math Phys. Eng. Sci.* 373, 20140159. doi: 10.1098/rsta.2014.0159

Singh, S., D'Sa, E., and Swenson, E. M. (2010). Chromophoric dissolved organic matter (CDOM) variability in Barataria Basin using excitation-emission matrix (EEM) fluorescence and parallel factor analysis (PARAFAC). *Sc. Tot. Environ.* 408, 3211–3222. doi: 10.1016/j.scitotenv.2010.03.044

Stedmon, C. A., Amon, R. M. W., Rinehart, A. J., and Walker, S. A. (2011). The supply and characteristics of colored dissolved organic matter (CDOM) in the Arctic Ocean: Pan Arctic trends and differences. *Mar. Chem.* 124, 108–118. doi: 10.1016/j.marchem.2010.12.007

Stedmon, C. A., and Bro, R. (2008). Characterizing dissolved organic matter fluorescence with parallel factor analysis: a tutorial. *Limnol. Oceanogr. Methods* 6, 572–579. doi: 10.4319/lom.2008.6.572

Stedmon, C. A., Granskog, M. A., and Dodd, P. A. (2015). An approach to estimate the freshwater contribution from glacial melt and precipitation in East Greenland shelf waters using colored dissolved organic matter (CDOM). *J. Geophys. Res. Oceans* 120, 1107–1117. doi: 10.1002/2014JC010501

Stedmon, C. A., and Markager, S. (2001). The optics of chromophoric dissolved organic matter (CDOM) in the Greenland Sea: An algorithm for differentiation between marine and terrestrially derived organic matter. *Limnol. Oceanogr.* 46, 2087–2082. doi: 10.4319/lo.2001.46.8.2087

Stedmon, C. A., Markager, S., and Bro, R. (2003). Tracing dissolved organic matter in aquatic environments using a new approach to fluorescence spectroscopy. *Mar. Chem.* 82, 239–254. doi: 10.1016/S0304-4203(03)00072-0

Stedmon, C. A., Markager, S., and Kaas, H. (2000). Optical properties and signatures of Chromophoric Dissolved Organic Matter (CDOM) in Danish coastal waters. *Estuarine Coast. shelf Sci.*, 267–278. doi: 10.1006/ecss.2000.0645

Stedmon, C. A., and Nelson, N. B. (2015). "The Optical Properties of DOM in the Ocean," in *Biogeochemistry of Marine Dissolved Organic Matter*. Eds. D. A. Hansell and C. A. Carlson (Academic Press, Amsterdam, Boston), 480–508.

Stoń-Egiert, J., and Kosakowska, A. (2005). RP-HPLC determination of phytoplankton pigments – comparison of calibration results for two columns. *Mar. Biol.* 147, 251–260.

Stoń-Egiert, J., Łotocka, M., Ostrowska, M., and Kosakowska, A. (2010). The influence of biotic factors on phytoplankton pigment composition and resources in Baltic ecosystems: new analytical results. *Oceanologia* 52, 101–125. doi: 10.5697/oc.52-1.101

Stubbins, A., Lapierr, J.-F., Berggren, M., Prairie, Y. T., Dittmar, T., and del Giorgio, P. A. (2014). What's in an EEM? Molecular signatures associated with dissolved organic fluorescence in boreal Canada. *Environ. Sci. Technol.* 48, 10598–10606. doi: 10.1021/es502086e

Tang, C. C. (2004). The circulation, water masses and sea ice of Baffin Bay. *Prog. Oceanogr.* 63, 183–228. doi: 10.1016/j.pocean.2004.09.005

Traganza, E. D. (1969). Fluorescence excitation and emission spectra of dissolved organic matter in the sea water. *Bull. Mar. Sci.* 19, 897–904.

Vonk, J. E., and Gustafsson, O. (2013). Permafrost-carbon complexities. *Nat. Geosci.* 6, 675–676. doi: 10.1038/ngeo1937

Wang, X., Zhang, F., Kung, H.–T., Ghulam, A., Trumbo, A. L., Yang, J., et al. (2017). Evaluation and estimation of surface water quality in an arid region based on EEM-PARAFAC and 3D fluorescence spectral index: a case study of the Ebinur Lake Watershed, China. *Catena* 155, 62–74. doi: 10.1016/j.catena.2017.03.006

Yamashita, Y. M., Jones, D. L., and Fuller, M. T. (2003). Orientation of asymmetric stem cell division by the APC tumor suppressor and centrosome. *Science* 301, 1547–1550. doi: 10.1126/science.1087795

Yamashita, Y., and Tanoue, E. (2003). Chemical characterization of protein-like fluorophores in DOM in relation to aromatic amino acids. *Mar. Chem.* 35, 255–271. doi: 10.1016/S0304-4203(03)00073-2

Zabłocka, M., Kowalczuk, P., Meler, J., Peeken, I., Dragańska-Deja, K., and Winogradow, A. (2020). Compositional differences of fluorescent dissolved organic matter in Arctic Ocean spring sea ice and surface waters north of Svalbard. *Mar. Chem.* 227, 103893. doi: 10.1016/j.marchem.2020.103893

Zimov, S. A., Davydov, S. P., Zimova, G. M., Davydova, A. I., Schuur, E. A. G., Dutta, K., et al. (2006). Permafrost carbon: Stock and decomposability of globally significant carbon pool. *Geophys. Res. Lett.* 33, 20. doi: 10.1029/2006GL027484

Zsolnay, A., Baigar, E., Jimenez, M., Steinweg, B., and Saccomandi, F. (1999). Differentiating with fluorescence spectroscopy the sources of dissolved organic matter in soils subjected to drying. *Chemosphere* 38, 45–50. doi: 10.1016/S0045-6535(98)00166-0